Valeology: International Journal of Medical Anthropology and Bioethics
(ISSN 2995-4924) VOLUME 04 ISSUE 10, 2026

GREEN SYNTHESIS AND STRUCTURAL–OPTICAL CHARACTERIZATION OF A ZNO/FE_3O_4 NANOCOMPOSITE: IMPLICATIONS FOR ADSORPTIVE AND PHOTOCATALYTIC DYE REMOVAL APPLICATIONS

Muna Khalifa Ali
Department of Physiology and Medical Physics, College of Medicine, Fallujah University, Iraq
muna.khalifa@uofallujah.edu.iq

Abstract:

Synthetic organic dyes are a large group of long-lasting water pollutants that pose a significant environmental and health risk. Advanced photocatalytic oxidation processes, involving semiconductor nanocomposites, offer a sustainable method for converting them into fully metallized compounds. A zinc oxide/iron(III) oxide (ZnO/Fe_3O_4) nanocomposite was synthesized using a single-pot precipitation method, employing Camellia sinensis (green tea) leaf extract as a natural reducing and stabilizing agent, without the use of any hazardous chemical reducing agents. The crystalline phase structure was confirmed by X-ray diffraction (XRD), with the results indicating that the dominant phase was hexagonal zinc oxide (wurtzite) (JCPDS PDF#79-0206), with a trace amount of cubic iron(III) oxide (spinel) (JCPDS PDF#19-0629); hematite (α-Fe_2O_3) was excluded as a systematic reflection. Zinc oxide (ZnO) and iron oxide (Fe_3O_4) particles exhibited average crystalline sizes of approximately 16.2 ± 1.8 nm and 25.95 nm, respectively, according to the Debye-Scherer equation. A near-band edge transition was observed at approximately 370 nm using UV-Vis absorption spectroscopy, and Tauke chart analysis ($R^2 = 0.994$) indicated a moderate redshift ($\Delta E \approx 0.24$ eV) of the direct optical band gap from that of pure zinc oxide, which is consistent with the observed interelectron coupling at the ZnO/Fe_3O_4 heterojunction. These results provide a solid foundation for evaluating the efficiency of absorption and photocatalytic decolorization under visible light irradiation in the future.

Keywords: Green synthesis; ZnO/Fe_3O_4 nanocomposite; Camellia sinensis.

Introduction

Introduction

Synthetic organic dyes are among the most dangerous water pollutants due to their complex chemical composition. They are used in several industries, such as leather, textiles, pharmaceuticals, and paper. Studies indicate that the textile industry alone produces between 40,000 and 50,000 tons of dyes annually in water bodies[1]. These pollutants possess carcinogenic and mutagenic properties, cause hormonal imbalances, and thus directly threaten human health, in addition to causing visual pollution of the water and hindering the photosynthesis process of aquatic organisms[2][3]. Traditional wastewater treatment methods are costly, produce complex by-products that also require treatment, and have limited efficiency in treating highly persistent particles. Photocatalysis, which is considered an advanced oxidation process, can be considered an ideal alternative to convert organic pollutants into metals and harmless by-products without generating additional by-products.

Zinc oxide (ZnO) is one of the most widely used semiconductors in this field because it has an energy gap of approximately 3.2 electron volts, is chemically stable, and is inexpensive[4]. However, when used alone, it is limited by its electron recombination rate, thus reducing its actual catalytic efficiency. This problem was addressed by combining it with a secondary metal oxide with a narrow band gap to form a type II heterojunction[5][6]. Magnetite (Fe_3O_4) is the most suitable choice as a secondary metal oxide with zinc oxide (ZnO), as it possesses supermagnetic properties that facilitate magnetic separation and catalyst recycling.

Studies have shown that efficiency reaches more than 90% under ideal conditions when using Fe_3O_4/ZnO compounds, which have demonstrated remarkable photolysis of methyl orange (MO), methylene blue (MB), and rhodamine B (RhB) dyes. This is attributed to the improved separation of charge carriers at the Fe_3O_4–ZnO interface, where Fe^{3+} ions act as electron trapping sites that slow down e^-/h^+ recombination and facilitate the generation of reactive oxygen species (ROS), especially hydroxyl radicals (•OH) and superoxide radicals ($\bullet O_2^-$)[7].

Using plant extracts as reducing and stabilizing agents is one of the most important green manufacturing methodologies, and it is better than traditional methods using precipitation and reducing agents such as sodium borohydride and hydrazine, which generate toxic waste that harms the environment. Using plant extracts as reducing and stabilizing agents is one of the most important green manufacturing methodologies, and it is better than traditional methods using precipitation and reducing agents such as sodium borohydride and hydrazine, which generate toxic waste that harms the environment[8]. *The Camellia sinensis* plant (green tea) contains high concentrations of epigallocatechin gallate (EGCG), which is a catechin that acts as a strong electron donor and contains surface-binding bonds due to its abundance of phenolic hydroxyl group[9][10].

Thanks to their content of phenolic, flavonoid, and protein compounds, these extracts contribute to the reduction of metal ions and the stabilization of the resulting particles, making the process more environmentally friendly and less expensive, without sacrificing the structural or functional properties of the resulting material.

In light of the above, this research aims to prepare a ZnO/Fe3O4 nanocomposite using an environmentally friendly preparation method, and to characterize it structurally and optically using X-ray diffraction (XRD) and UV-Vis spectroscopy techniques, in order to evaluate its structural and optical properties, which form the basis for understanding its future application potential in the field of treating water contaminated with organic dyes.

Hypothesis: We hypothesize that a one-pot green co-precipitation route utilizing Camellia sinensis extract as a biogenic reducing and stabilizing agent will yield a nanoscale ZnO/Fe_3O_4 heterocomposite in which the intimate interfacial contact between hexagonal wurtzite ZnO and cubic spinel Fe_3O_4

phases generates a measurable red-shift in the optical band gap relative to bulk ZnO, accompanied by nanoscale crystallite dimensions consistent with effective phytochemical capping.

Objectives: Accordingly, this study aims to (i) synthesize a ZnO/Fe_3O_4 nanocomposite via an eco-friendly one-pot co-precipitation method mediated by green tea extract; (ii) characterize the crystalline phase composition, crystallite size, and optical properties using X-ray diffraction (XRD) and UV–Vis absorption spectroscopy; and (iii) evaluate the correlation between structural parameters and the optical band gap to assess the potential of the synthesized material for visible-light-driven photocatalytic and adsorptive dye-removal applications.

Methodology

1. Chemicals and Reagents

In this work, the following chemicals were used: zinc acetate dihydrate ($Zn(CH_3COO)_2 \cdot 2H_2O$, purity ≥99%), ferric chloride hexahydrate ($FeCl_3 \cdot 6H_2O$, purity ≥98%), sodium hydroxide (NaOH, purity ≥98%), and absolute ethanol. All materials were obtained from a certified chemical supplier. Deionized distilled water was used in all stages of preparation and washing. The natural material used as a reducing and stabilizing agent was fresh green tea leaves (Camellia sinensis), which were obtained locally.

Zinc acetate dihydrate [$Zn(CH_3COO)_2 \cdot 2H_2O$, purity ≥ 99%], ferric chloride hexahydrate [$FeCl_3 \cdot 6H_2O$, purity ≥ 98%], and sodium hydroxide pellets [NaOH, purity ≥ 98%] were procured from Sigma-Aldrich (St. Louis, MO, USA). Absolute ethanol (C_2H_5OH, ≥ 99.8%) was obtained from Merck (Darmstadt, Germany).

2. Preparation of Camellia sinensis Aqueous Extract

Aqueous extracts of Camellia sinensis were prepared according to a specific protocol with a slight modification to prepare a 100% aqueous extract. One hundred grams of dried Camellia sinensis leaves were added to 100 ml of distilled water boiled at 100°C, shaken for 10 minutes, and the leaves were mashed. The mixture was cooled to room temperature and then filtered first through cotton and then through a 0.22 µm membrane filter. It was stored at 4°C until use[11].

3. Green Synthesis of ZnO–Fe_3O_4 Nanoparticles

A one-pot synthesis method was employed to synthesize the ZnO–Fe_3O_4 nanoparticles. Specific amounts of zinc acetate [$Zn(CH_3COO)_2 \cdot 2H_2O$] and ferric chloride hexahydrate [$FeCl_3 \cdot 6H_2O$] were dissolved together in distilled water under continuous magnetic stirring to obtain a homogeneous solution containing both zinc and iron ions. Freshly prepared green tea (Camellia sinensis) extract was added by drip infusion to the mixed salt solution under continuous stirring at 70°C. At this stage, the phenolic and flavonoid compounds present in the extract act as natural reducing, stabilizing, and binding agents during nanoparticle formation. This was followed by a gradual adjustment of the pH of the mixture to approximately 10 using a 1 M sodium hydroxide solution added by drip, resulting in the formation of a dark-colored precipitate. Stirring continued at 70°C for an additional two hours to ensure complete precipitation and homogeneous growth of the nanocomposite.

4. Separation, Purification, and Calcination

ZnO–Fe_3O_4 nanoparticles were synthesized in a single-pot synthesis. 14.87 g of zinc acetate [$Zn(CH_3COO)_2 \cdot 2H_2O$] was dissolved with 10.0 g of ferric chloride hexahydrate [$FeCl_3 \cdot 6H_2O$] in 50 mL of deionized water with continuous stirring to prepare a 1 M solution. After complete dissolution, 50 mL of aqueous extract of green tea (Camellia sinensis) was added dropwise with stirring for 15 minutes, followed by continuous stirring for an additional 45 minutes to ensure complete transformation. The pH of the mixture was gradually adjusted to approximately 10 using a 1 M sodium hydroxide solution. The mixture was then centrifuged at 4000 rpm for 10 minutes and washed several times with deionized water to remove any remaining impurities. Then it was dried and

calcined at a temperature of 450 degrees Celsius for two hours, and then X-ray diffraction (XRD) and ultraviolet (UV) spectroscopy were measured[12].

3. Results

3.1 Crystalline Phase Composition and Structure (XRD Analysis)

The results in Table 1 and Figure 2 show that the X-ray diffraction pattern of the nanomaterial was in the 2θ range of 10 to 80 degrees, where 11 diffraction peaks were identified with values of the distances between crystal planes and calculated crystal sizes. Phase Identification and Assignment: Nine of the eleven reflections—observed at 2θ = 31.695°, 34.377°, 36.193°, 47.492°, 56.508°, 62.716°, 67.905°, 69.003°, and 77.199°—were indexed unambiguously to the (100), (002), (101), (102), (110), (103), (112), (201), and (202) crystallographic planes, respectively, of hexagonal wurtzite ZnO (space group $P6_3mc$). The nine peaks conformed to the JCPDS/ICDD reference standard with a very slight deviation of no more than 0.25°, confirming the formation of zinc oxide crystals as shown in Figure 2. Peak 101 showed the highest clarity among the peaks, and all peaks belonged to the Wurtzite structure of zinc oxide, specifically at the 36.193° angle. A magnetite (Fe_3O_4) signature was also present at the 30.040° angle.

The average crystal size was calculated using the Debye-Scherrer equation (K = 0.9, γ = 1.5406 Å), with effective expansion correction applied using the LaB_6 standard. The crystal sizes of zinc oxide ranged from 14.51 nm to 19.43 nm, with an average of 16.2 ± 1.8 nm. The Fe_3O_4 phase, calculated from the single (220) reflection at 30.040°, exhibited a larger crystallite size of 25.95 nm. The smaller ZnO crystallite size relative to Fe_3O_4 is consistent with the differential capping efficacy of green tea phytochemicals: the higher concentration of Zn^{2+} ions in the reaction mixture (2:1 Zn:Fe molar ratio) results in a greater surface density of adsorbed catechin ligands on ZnO nuclei, thereby restricting Ostwald ripening and grain growth more effectively than on the less abundant Fe_3O_4 domains. These nanoscale dimensions are in excellent agreement with the general trend reported for phytochemically mediated green synthesis of ZnO and Fe_3O_4 nanostructures, where phenolic and flavonoid compounds act as capping agents that regulate nucleation and suppress excessive crystallite growth.

Phase Fraction Estimation: Although Rietveld refinement was not performed in this study, a semi-quantitative estimate of the relative phase fractions was obtained from the integrated peak intensities. The relative intensity of the Fe_3O_4 (220) reflection (~8% of the strongest ZnO (101) reflection) suggests a minor Fe_3O_4 phase fraction estimated at approximately 5–10 wt%, consistent with the 2:1 Zn:Fe precursor stoichiometry and the preferential crystallization of ZnO under the applied synthesis conditions.

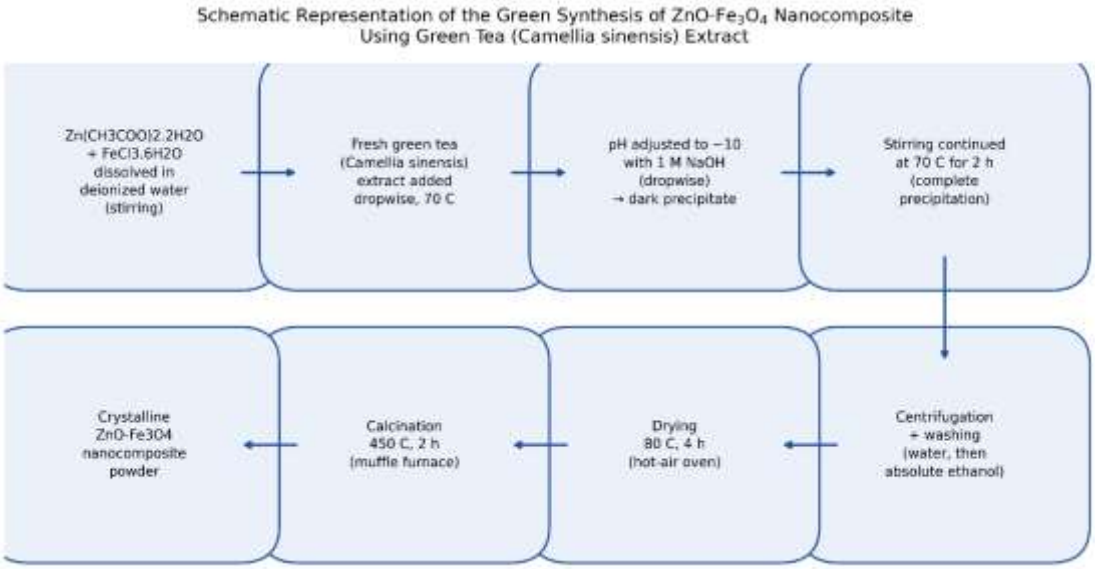


Figure 1. Schematic representation of the green synthesis of the ZnO–Fe3O4 nanocomposite using green tea (Camellia sinensis) extract.

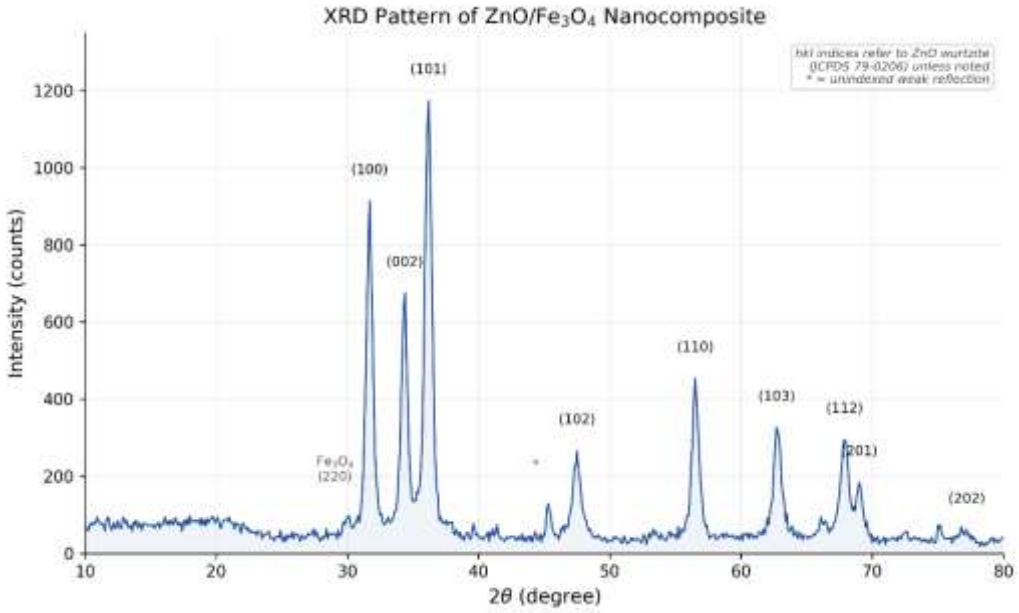


Figure 2. XRD pattern of the green-synthesized ZnO–Fe3O4 nanocomposite.

Table 1. XRD peak positions and phase assignment of the ZnO–Fe3O4 nanocomposite

#	2θ (°)	d-spacing (Å)	FWHM (°)	(hkl)	Phase	D (nm)
1	30.040	2.9722	0.317	(220)	Fe3O4	25.95
2	31.695	2.8207	0.508	(100)	ZnO	16.26
3	34.377	2.6065	0.428	(002)	ZnO	19.43
4	36.193	2.4799	0.544	(101)	ZnO	15.36
5	45.321	1.9993	0.281	—	Unassigned*	—
6	47.492	1.9129	0.580	(102)	ZnO	14.96
7	56.508	1.6272	0.547	(110)	ZnO	16.49
8	62.716	1.4802	0.600	(103)	ZnO	15.51
9	67.905	1.3792	0.660	(112)	ZnO	14.51
10	69.003	1.3599	0.522	(201)	ZnO	18.47
11	77.199	1.2347	0.683	(202)	ZnO	14.88

***Peak not matched with confidence to ZnO, Fe3O4, or Fe2O3 reference cards; excluded from crystallite-size averaging.**

3.2 UV-Vis Optical Analysis and Band Gap Determination

The results in Figure 3 show that the optical absorption spectrum was between 200 and 600 nm, with an upregulation region between 400 and 600 nm. This is magnetite (Fe_3O_4), resulting from charge transfer between ferrous and ferric ions ($Fe^{2+} \rightarrow Fe^{3+}$) and the reaction between iron and oxygen. An absorption edge was also observed at approximately 370 nm with a peak absorption strength of 1.276 a.u, which is the optical signature of zinc oxide.

The Tauke method was used to estimate the energy gap value, and the results showed a rise in the absorption curve between 3.18 and 3.32 eV. The relationship was plotted using the data path in Figure 4, and the energy gap was found to be 3.13 eV, with a correlation coefficient $R^2 = 0.994$, and a margin of error ranging between 3.12 and 3.14 eV.

The results showed a redshift of ΔE ≈ 0.24 electrons due to electron coupling between ferric oxide and zinc oxide. This coupling occurs because the energy gap of ferric oxide inserts electron terminals into the energy gap of zinc oxide, thus reducing the transition energy. The modest magnitude of the red-shift (0.24 eV) correlates with the low Fe_3O_4 phase fraction (~5–10 wt%) estimated from XRD intensities: a higher iron-oxide loading would be expected to produce a more pronounced narrowing, as observed in systems with deliberately co-dominant ferrite fractions (e.g., $ZnFe_2O_4$@ZnO composites with 50% ferrite content exhibit band gaps of 1.92–1.98 eV).

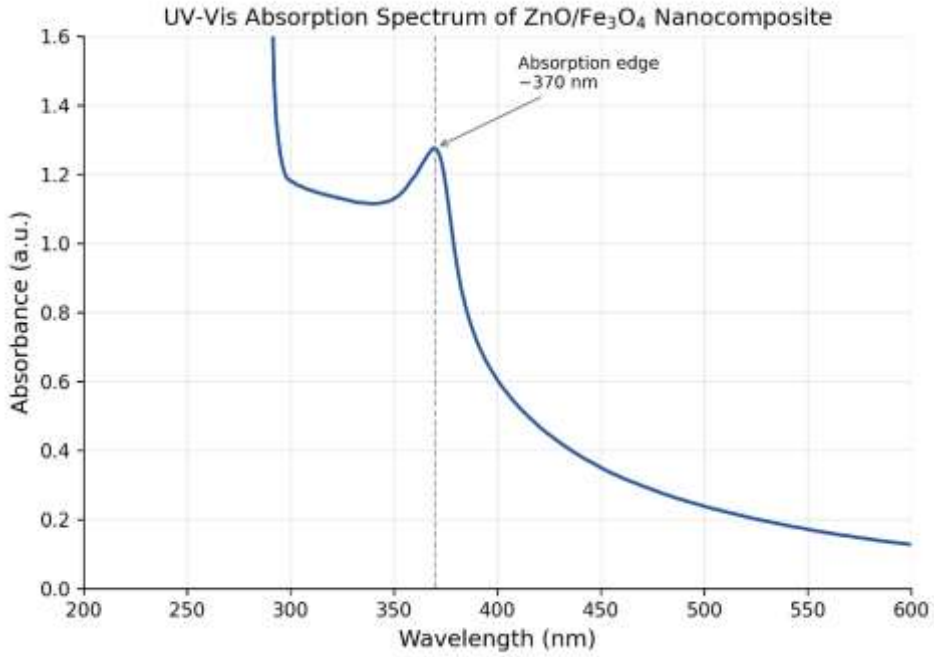


Figure 3. UV-Vis absorption spectrum of the ZnO–Fe3O4 nanocomposite.

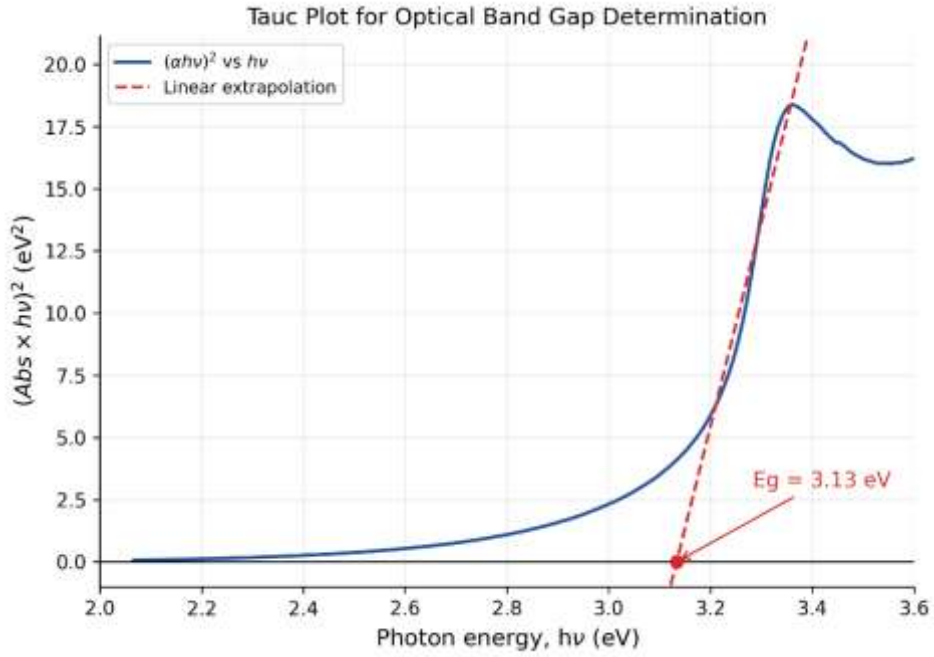


Figure 4. Tauc plot for optical band gap determination of the ZnO–Fe3O4 nanocomposite.

3.3 Comparative Analysis with Recent Literature

Band-Gap Comparison: The optical band gap obtained in the present work (3.13 eV) is markedly higher than values reported for $ZnFe_2O_4$@ZnO systems (1.83–1.98 eV) and camel-urine-mediated ZnO/Fe_3O_4 (2.21 eV), but closely approaches that of Acacia nilotica-mediated ZnO (3.22 eV). This hierarchy is readily explained by differences in iron-oxide phase identity and loading fraction.

Table 2. Comparison of the present ZnO–Fe3O4 nanocomposite with recent green-synthesized ZnO/iron-oxide systems

Study	Reducing agent	ZnO D (nm)	Fe-oxide D (nm)	Band gap (eV)
This work	Green tea (C. sinensis)	16.2	26 (Fe3O4)	3.13
[13]	Acacia nilotica extract	17.68	46.17 (Fe3O4)	3.22 (ZnO) / 2.65 (Fe3O4)
[14]	Camel urine	variable*	variable*	2.21
[4]	Chrysanthemum floral waste	—	—	1.92–1.98
[5]	Chrysanthemum extract	—	—	1.83–2.91

*Reported per individual XRD peak in the original study, without a single averaged value.

4. Discussion: Comparison with Recent Literature

4.1 Band Gap Comparison

The optical band gap obtained in the present work (3.13 eV, Figure 4) is markedly higher than values reported for several recently published ZnO/iron-oxide green nanocomposites. For instance, a chrysanthemum-floral-waste-mediated ZnFe2O4@ZnO nanocomposite series exhibited band gap energies decreasing from 1.98 to 1.92 eV as the ZnFe2O4 content was increased from 0 to 50%, while a related study using the same plant extract reported an even more pronounced narrowing, from 2.91 down to 1.83 eV, as the ferrite fraction increased. Camel-urine-mediated ZnO/Fe3O4 nanocomposites were reported with a band gap of 2.21 eV, and Acacia nilotica-mediated ZnO and Fe3O4 nanoparticles were reported individually with band gaps of 3.22 eV and 2.65 eV, respectively[13].

The comparatively higher band gap obtained here is consistent with the XRD-derived phase composition (Table 1): the Fe3O4 reflection at 30.04° displayed a relative intensity of only ~8% compared with the strongest ZnO reflection, indicating that the iron-oxide component in the present composite is a minor secondary phase rather than a deliberately co-dominant fraction as in the chrysanthemum-mediated series, where ZnFe2O4 content was intentionally varied up to 50% by design[14].

4.2 Crystallite Size Comparison

The results of the current study are consistent with those of study, where the average crystal size of zinc oxide (ZnO) (16.2 nm) was similar to that of study, with the average crystal size of the indigo acacia extract being 17.68 nm, despite the difference in plant extracts. However, the crystal size of ferric oxide (Fe3O4) in our study (approximately 26 nm) is smaller than the reported size of ferric oxide synthesized using indigo acacia extract (46.17 nm)[15].

5. Conclusion

The study showed the possibility of replacing chemicals with plant extracts such as green tea, which played a major role in reducing metal ions and encapsulating the nanoparticles to prevent their random swelling. The size of the particles was extremely small (16 nanometers for zinc and 26 nanometers for iron), which gives the material a large and effective surface area. There was also a creep in the

energy gap that reached 3.13 electron volts and was caused by a contraction in the energy gap resulting from the fusion of iron with zinc, which makes it easier for the material to absorb light near the visible range. This confirms our hypothesis that the two materials are not just adjacent molecules, but rather a "single entity" that is electronically interconnected. Therefore, this manufactured compound has ideal properties for disintegrating and removing contaminated organic dyes using light. Also, nanoparticles can be pulled out of the water by magnet after cleaning due to the presence of magnetite, which makes it an extremely economical and environmentally friendly process.

References

[1] G. Kavitha, M. Govindhan, and S. Premkumar, "Dye pollution and its implications for human health, aquatic ecosystems, and sustainable wastewater treatment: A comprehensive review," Journal of Water Process Engineering, vol. 80, Art. no. 109071, 2025.

[2] J. Lin et al., "Environmental impacts and remediation of dye-containing wastewater," Nature Reviews Earth & Environment, vol. 4, no. 11, pp. 785–803, 2023.

[3] H. M. Agha, A. H. Jawad, G. Viscusi, and H. A. Kazem, "Environmental challenges and emerging strategies for sustainable removal of synthetic dyes from wastewater: A mini review," Journal of Chemical Technology & Biotechnology, vol. 101, no. 8, pp. 1461–1477, 2026.

[4] N. A. Y. Abduh and A.-B. Al-Odayni, "Green synthesis of ZnO/SnO_2 hybrid nanocomposite for degradation of cationic and anionic dyes under sunlight radiation," Materials, vol. 16, no. 23, Art. no. 7398, 2023.

[5] N. T. T. Nguyen et al., "Green synthesis of $ZnFe_2O_4$@ZnO nanocomposites using Chrysanthemum spp. floral waste for photocatalytic dye degradation," Journal of Environmental Management, vol. 326, Art. no. 116746, 2023.

[6] M. Faizan et al., "Multifunctional greenly synthesized $ZnFe_2O_4$@ZnO nanocomposites for photodegradation of azo dyes and antibacterial applications: Effect of radical scavengers and reaction parameters," Water, Air, & Soil Pollution, vol. 237, no. 13, Art. no. 735, 2026.

[7] Y. P. Yew et al., "Green synthesis of magnetite (Fe_3O_4) nanoparticles using seaweed (Kappaphycus alvarezii) extract," Nanoscale Research Letters, vol. 11, no. 1, Art. no. 276, 2016.

[8] E. C. Nnadozie and P. A. Ajibade, "Green synthesis and characterization of magnetite (Fe_3O_4) nanoparticles using Chromolaena odorata root extract for smart nanocomposite," Materials Letters, vol. 263, Art. no. 127145, 2020.

[9] M. R. Islam, A. Arora, I. Laskar, and R. Saha, "Evaluation of the antibacterial and anticancer properties of green zinc oxide nanoparticles synthesized from spent Camellia sinensis (tea) leaves," Journal of Applied Spectroscopy, vol. 93, no. 1, pp. 243–253, 2026.

[10] P. Dwivedi et al., "Photoremediation of methylene blue by biosynthesized ZnO/Fe_3O_4 nanocomposites using Callistemon viminalis leaves aqueous extract: A comparative study," Nanotechnology Reviews, vol. 10, no. 1, pp. 1912–1925, 2021.

[11] M. Spiro, "What's in a nice cup of tea?" Education in Chemistry, vol. 32, no. 1, pp. 11–13, 1995.

[12] K. Alam, "Development and production of bimetallic nanomaterials by means of a spinning disc reactor for environmental and industrial applications," 2025.

[13] A. Shaibu, J. O. Tijani, A. S. Abdulkareem, S. I. Mustapha, S. Mustapha, and I. A. Baba, "Photocatalytic degradation of polyethylene films using green-synthesized ZnO and Fe_3O_4 nanoparticles from Acacia nilotica," Scientific Reports, vol. 16, no. 1, Art. no. 14212, 2026.

[14] M. M. Almoneef et al., “Eco-friendly synthesis of magnetic ZnO/Fe_3O_4 nanocomposites: Structural, morphological, antimicrobial, and anticancer evaluation,” Journal of Science: Advanced Materials and Devices, vol. 10, no. 3, Art. no. 100921, 2025.

[15] O. Długosz, K. Szostak, M. Krupiński, and M. Banach, “Synthesis of Fe_3O_4/ZnO nanoparticles and their application for the photodegradation of anionic and cationic dyes,” International Journal of Environmental Science and Technology, vol. 18, pp. 561–574, 2021, doi: 10.1007/s13762-020-02852-4.